atmosphere

MDPI

Article

Examination of WRF-ARW Experiments Using Different Planetary Boundary Layer Parameterizations to Study the Rapid Intensification and Trajectory of Hurricane Otto (2016)

Tito Maldonado [1,*], Jorge A. Amador [1,2], Erick R. Rivera [1,2], Hugo G. Hidalgo [1,2] and Eric J. Alfaro [1,2,3]

1 Center for Geophysical Research, University of Costa Rica, San Jose 11501, Costa Rica; jorge.amador@ucr.ac.cr (J.A.A.); erick.rivera@ucr.ac.cr (E.R.R.); hugo.hidalgo@ucr.ac.cr (H.G.H.); erick.alfaro@ucr.ac.cr (E.J.A.)
2 School of Physics, University of Costa Rica, San Jose 11501, Costa Rica
3 Center for Research in Marine Sciences and Limnology, University of Costa Rica, San Jose 11501, Costa Rica
* Correspondence: tito.maldonado@ucr.ac.cr

Received: 30 October 2020; Accepted: 23 November 2020; Published: 4 December 2020

Abstract: Hurricane Otto (2016) was characterised by remarkable meteorological features of relevance for the scientific community and society. Scientifically, among the most important attributes of Otto is that it underwent a rapid intensification (RI) process. For society, this cyclone severely impacted Costa Rica and Nicaragua, leaving enormous economic losses and many fatalities. In this study, a set of three numerical simulations are performed to examine the skill of model estimations in reproducing RI and trajectory of Hurricane Otto by comparing the results of a global model to a regional model using three different planetary boundary layer parameterizations (PBL). The objective is to set the basis for future studies that analyse the physical reasons why a particular simulation (associated with a certain model setup) performs better than others in terms of reproducing RI and trajectory. We use the regional model Weather Research and Forecasting—Advanced Research WRF (WRF-ARW) with boundary and initial conditions provided by the Global Forecast System (GFS) analysis (horizontal resolution of 0.5 degrees). The PBL used are the Medium Range Forecast, the Mellor-Yamada-Janjic (MYJ), and the Yonsei University (YSU) parameterizations. The regional model is run in three static domains with horizontal grid spacing of 27, 9 and 3 km, the latter covering the spacial extent of Otto during the simulation period. WRF-ARW results improve the GFS forecast, in almost every aspect evaluated in this study, particularly, the simulated trajectories in WRF-ARW show a better representation of the cyclone path and movement compared to GFS. Even though the MYJ experiment was the only one that exhibited an abrupt 24-h change in the storm's surface wind, close to the 25-knot threshold, the YSU scheme presented the fastest intensification, closest to reality.

Keywords: WRF; tropical cyclones; natural hazards; regional numerical modelling; Costa Rica; Central America

1. Introduction

Southern Central America (i.e., Costa Rica and Panama) is rarely affected by the direct impact of hurricanes [1,2]. The regions where tropical cyclones form in the Atlantic and Caribbean Sea and their usual northeastward trajectories are the two main reasons that prevent these systems from reaching the southern subregion. On 23–25 November 2016, however, Hurricane Otto formed near the Caribbean coast of Panama and later hit Nicaragua and Costa Rica. According to the records of the

National Oceanographic and Atmospheric Administration (NOAA) of the United States of America (USA), Otto was the southernmost hurricane to make landfall in Central America [3]. Previously, nearby northern Costa Rica, observational records show that Hurricane Irene (1971) is the closest landfalling hurricane to Otto. In fact, Irene made landfall in southern Nicaragua at about 25–30 nautical miles (n mi) north of Otto's position [4]. In addition, Otto is the only known hurricane to move over Costa Rica. It is noteworthy that there is evidence of at least two more landfalling tropical cyclones in southeastern Central America (i.e., Costa Rica and Panama): they are Tropical Storm 19 in 1887 [5] and Martha in 1969 [6]. Furthermore, according to Brown's report [3]: Hurricane Otto underwent a rapid intensification (hereafter, RI) process before landfall. As was observed, the hurricane intensified from category 1 to 3, having a change of 35 knots (17.5 m s^{-1}) in the surface wind in less than 18 h in agreement with the definition of RI by Kaplan and DeMaria [7].

According to Kaplan and DeMaria [7] "the unexpected RI of hurricanes so close to the coast underscores the need for improving our understanding of TC intensification". For society, coastal populations can experience enormous economic losses and many fatalities. In this study, a set of three numerical simulations are performed to examine the skill of model estimations of reproducing RI and trajectory of Hurricane Otto by comparing the results of a global model to a regional model using three different boundary layer parameterizations. The objective is to set the basis for future studies that analyse the physical reasons why a particular simulation (associated with a certain model setup) performs better than others in terms of reproducing RI and trajectory.

In Figure 1a the storm track from the National Hurricane Center Best Track (BT) data is shown. The time series of both maximum sustained winds and central pressure for Otto are presented in Figure 1b. Tracking started on 17 November 2016 (1800 UTC) when Otto was still a low pressure (L) system (dashed green line). It became a tropical depression (TD) at 1800 UTC 20 November 2016 (solid green line), and later a tropical storm (TS) at 0600 UTC 21 November 2016 (solid yellow line). Otto reached for the first time the status of hurricane category 1 (H1) at 1800 UTC 23 November 2016 (solid red line), category 2 (H2) at 0600 UTC 24 November 2016 (dashed red line), and category 3 (H3) at 1200 UTC 24 November 2016 (solid pink line). It made landfall over the Caribbean coast of Nicaragua as H3 at approximately 1730 UTC 24 November 2016, reaching maximum sustained winds of 51.4 m s^{-1} and central pressure values of 975 hPa (Figure 1b). After landfall, it lost strength and became H2 status at 1800 UTC 24 November 2016, and H1 at 0000 UTC 25 November 2016. It exited Costa Rica as a TS at 0330 UTC 25 November 2016. Otto became again a tropical depression at 1200 UTC 26 December 2016 and dissipated at 1800 UTC 26 December 2016. Figure 2 presents infrared (IR) satellite imagery of the evolution and movement of tropical cyclone Otto on 24 November 2016. A well-defined eye is observed during the periods of maximum intensity (Figure 2a,b). The landfall and inland penetration of the system are shown in Figure 2c,d. A detailed analysis of the lightning activity associated with the progress of Otto before and after landfall can be found in Arce-Fernández and Amador [8] using data from the World Wide Lightning Location Network (WWLLN, http://wwlln.net/). In this work, lightning associated with the rain bands of Otto, as observed from Infrared GOES-13 imagery (http://cimss.ssec.wisc.edu/goes/blog/archives/22683), was observed to be related to the intensification processes of this tropical cyclone.

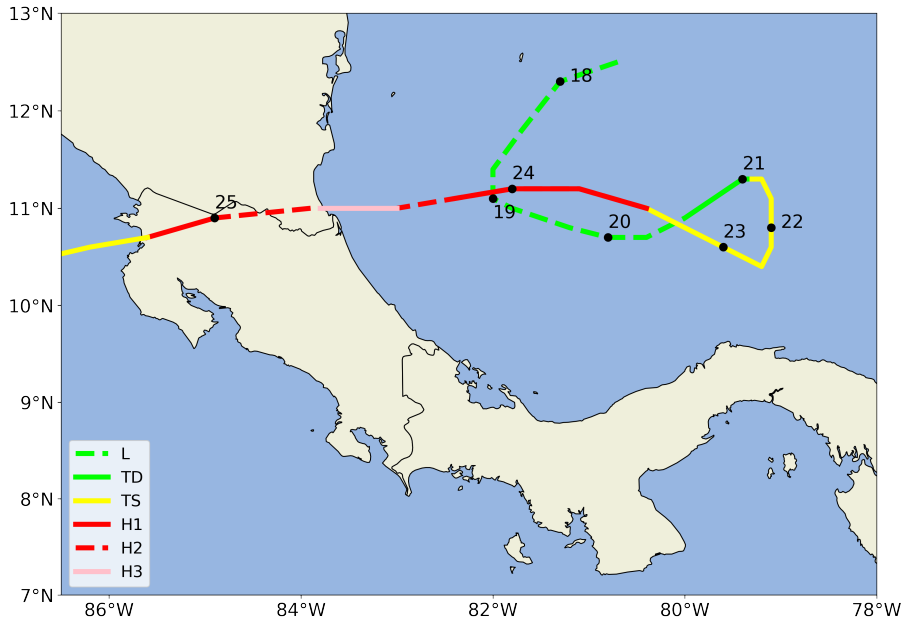

(**a**)

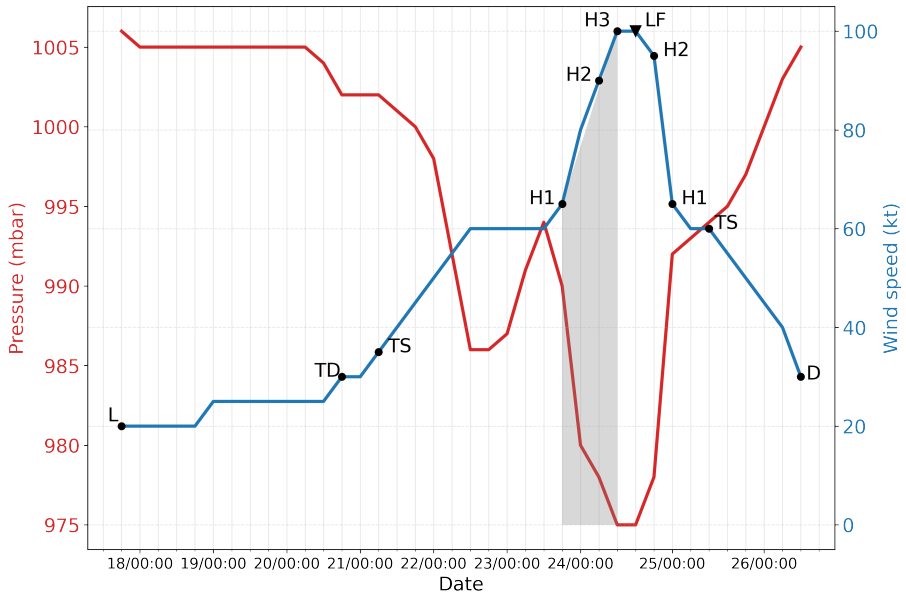

(**b**)

Figure 1. (**a**) Best Track of tropical cyclone Otto from 17 to 25 November 2016. The maximum sustained winds and the central pressure time series are presented in (**b**). The shaded area in (**b**) shows the RI period. The tropical cyclone evolution is indicated by L: low pressure, TD: tropical depression, TS: tropical storm, H1, H2, and H3: hurricane category 1, 2 and 3, LF: landfall and D: dissipation. The data in the x-axis is 6-h spaced, except for the points LF (24/1730 UTC) and TS (25/0330 UTC). Data source from Brown [3].

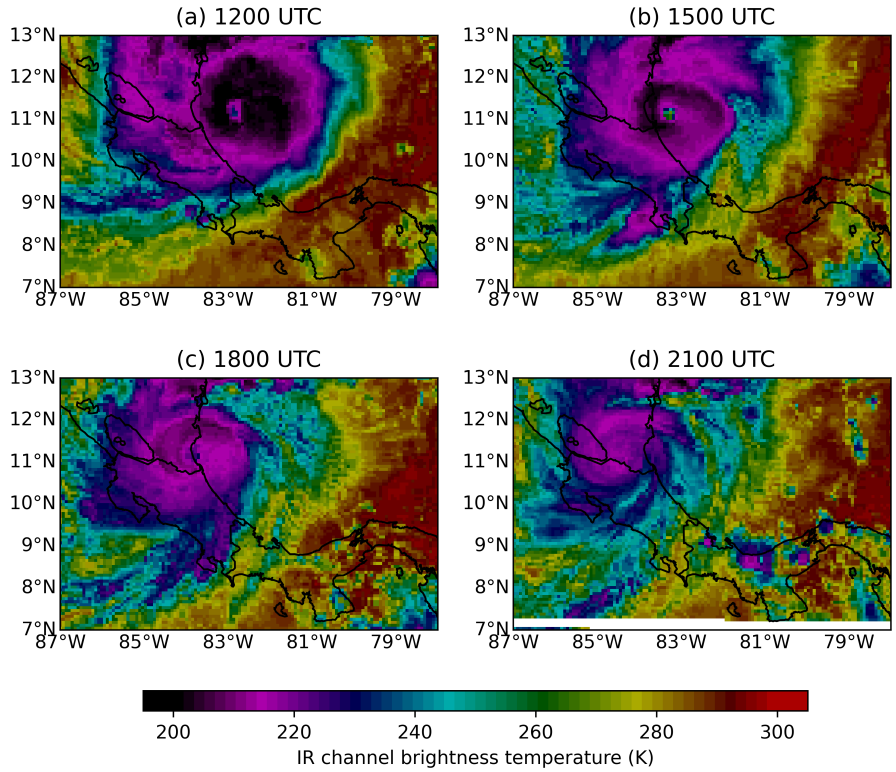

Figure 2. Infrared GOES-13 satellite imagery of tropical cyclone Otto at (**a**) 1200 UTC, (**b**) 1500 UTC, (**c**) 1800 UTC and (**d**) 2100 UTC 24 November 2016. (Data source: HURSAT, Knapp and Kossin [9]).

Hurricane Otto was characterised by remarkable meteorological features of interest for the scientific community. It is one of a small number of tropical cyclones that maintained hurricane status after moving from the Atlantic to the eastern North Pacific basin. Furthermore, this late-season hurricane set several historical records. It is the second latest hurricane to form in a calendar year over the Caribbean Sea (one day before Hurricane Martha in 1969), and is the strongest hurricane on record to form so late in the year. Also, Otto is the latest hurricane in documented history to be located on the Caribbean Sea, and its landfall on 24 November is the latest in the Atlantic basin in a calendar year [3]. Otto also underwent a RI process as seen in Figure 1b, given that the hurricane intensified from category 1 to 3 (35 knots or 17.5 m s^{-1}) in less than 18 h. According to Brown [3], this hurricane is responsible for 18 direct casualties. Widespread damage occured in southern Nicaragua and northern Costa Rica. In Panama, Costa Rica, and Nicaragua, the impacts of this tropical cyclone were severe, affecting nearly 25,000 people, and damaging more than 2400 homes [10]. Numerous homes, roads, and bridges were battered in Costa Rica. Thousands of people were left without fresh water supply after the storm passage due to power outages and damage of hundreds of water distribution systems. The National Meteorological Institute of Costa Rica (IMN in Spanish) reported that losses in road infrastructure and the coffee industry totalled approximately $15 million US dollars [11]. There are several recent studies showing Hurricane Otto impacts and their spatial distribution [10–15].

The importance of understanding an extreme RI event like the one shown by Otto, and the growing need to implement operational regional model systems in meteorological services of Central America, create the opportunity to investigate the ability of state-of-the-art regional and mesoscale models to represent the most relevant characteristics of this hurricane. To date, the only regional modelling study of Hurricane Otto was carried out by Poleo et al. [16]. Those authors analysed the performance of WRF-EMS (Weather Research and Forecasting - Environmental Model) in forecasting the evolution of Otto using different cumulus parameterizations. They found that the Grell-Freitas scheme [17] produced a better representation of the spatial and temporal distribution of precipitation, but they also highlighted the existence of a 2-h lag in the position of the modelled hurricane eye

with respect to observations. Poleo et al. [16], however, do not examine the RI observed during Otto evolution, nor the trajectory followed by this hurricane.

Since regional models can be valuable tools for predicting the landfall and intensification of tropical cyclones, the objective of this study is to examine the performance of WRF-ARW (Weather Research and Forecasting-Advanced Research WRF model version 3, Skamarock et al. [18]) using three different planetary boundary layer parameterizations in the estimation of Otto's trajectory and the RI process. In order to achieve this goal, the experiments were computed for the period spanning from 1200 UTC 23 November 2016 to 1200 UTC 25 November 2016. During this period the hurricane underwent a RI process, just before making landfall near the Biological Reserve Indio Maíz, in southeastern Nicaragua. In the rest of this section, we summarise previous RI cases over the Atlantic Ocean, and earlier studies that used numerical models to analyse the RI in hurricanes. In Section 2 a description of the data, methods and experimental setup carried out in this research is presented. Main results are commented on in Section 3. Lastly, Section 4 summarises our final remarks and conclusions of the study are presented in Section 5.

1.1. Previous Rapid Intensification Cases over the Atlantic Basin

Cases of tropical cyclone (TC) RI in the North Atlantic basin have been reported in several studies. According to Kaplan and DeMaria [7], Hurricanes Opal (1995) and Bret (1999) intensified rapidly before reaching the US coast and were responsible for large socio-economic impacts and loss of lives. From 1989 to 2000, they identified 159 RI events in 50 TCs (including non-developing tropical depressions). With respect to non-RI cases, the authors found that RI cases formed in regions with warmer sea surface temperature (SST), higher relative humidity (RH) at the lower troposphere, weaker vertical wind shear and more easterly upper-level flow. A follow-up study by Kaplan et al. [19] determined that most of the RI events happened in September, and that the number of occurrences was greater in the late hurricane season months than in earlier months.

In the period 1974–2010, Klotzbach [20] found about three times as many RI cases in the Atlantic basin during cold phases of the El Niño-Southern Oscillation (ENSO) compared to warm ENSO phases. In the same study, the Madden-Julian Oscillation (MJO) also exhibited influence on the number of RI cases. In phases 1–2 of the MJO more RI episodes occurred than in phases 6–7. Wang et al. [21] found, in the 1950–2014 period, 215 TCs (including tropical depressions) that experienced RI at least once. Like Kaplan et al. [19], they determined that most RI events occur in September. In addition, these authors identified three regions of maximum RI occurrence: (1) the western tropical North Atlantic, (2) the Gulf of Mexico and the western Caribbean Sea, and (3) the open ocean southeast and east of Florida, while the eastern Caribbean Sea is an area of minimum RI activity. Hurricane Otto is a clear example of a late-season rapidly intensifying TC that formed over one of the most favourable regions for RI processes. According to [3], high SST of 29 °C and moderate vertical wind shear favoured the strengthening of this system.

In the twenty-first century, two cases of TC RI, in addition to Otto, are remarkable. First, Hurricane Katrina (2005) was one the most powerful, deadliest and costliest tropical cyclones to impact the USA. It intensified from a Category 3 hurricane to a Category 5 in less than 12 h [22]. McTaggart-Cowan et al. [23] hypothesised that Katrina's RI was linked to its passage over a deep warm core ring in the Gulf of Mexico. Second, Hurricane Maria (2017), a major storm that caused severe damages in places such as Dominica, Puerto Rico and the USA, strengthened rapidly from category 3 to category 5 in only 12 h [24]. Pasch et al. [24] and Klotzbach et al. [25] indicate that this storm intensified in an environment of warm SST and low vertical wind shear.

1.2. Rapid Intensification, Storm Track and Boundary Layer in Regional Models

There are several proposed mechanisms to explain RI processes, most of which are related to boundary layer interactions, such as the positive feedback between convective heating around the vortex centre and vortex-scale motion [26–28], thermal wind balance with moisture in the eye

wall [29–31]. The planetary boundary layer (PBL) has been shown to play an important role in the spin-up of the tropical cyclone. Smith et al. [32] argued that enhanced angular momentum can occur in the PBL because of the strong inward flow. By comparing with aircraft observations, Zhang et al. [33] evaluated the effects of improved vertical diffusion on the simulated track, intensity, and structure of retrospective HWRF (Hurricane WRF) forecasts of four hurricanes. Their results showed better HWRF track and intensity forecasts in response to a more realistic representation of the PBL vertical diffusion. Kilroy et al. [34] studied the impact of surface drag on the intensification of TCs. They used a regional model for two idealised cases, one with friction and the other with zero surface drag. The vortex in the experiment without surface drag takes over twice as long to reach its intensification start time, in agreement with previous studies. Furthermore, the simulated inner core size of the vortex was considerably larger and weaker in intensity. Zhang et al. [35] found that for smaller eddy diffusivity (K_m), the simulations are in better agreement with the observations, improving the forecast of RI. It is found that the forecasts with reduced K_m at the RI onset have a shallower PBL with stronger inflow, more unstable near-surface air outside the eye wall, stronger and deeper updrafts in regions farther inward from the radius of maximum wind (RMW), and stronger PBL convergence closer to the storm centre, although the mean storm intensity (as measured by the 10-m winds) is similar for the two groups.

The above studies highlight the crucial role that PBL processes play in changing the intensity, structure and trajectory of TCs. Therefore, this work examines the representation of Hurricane Otto's RI in the WRF-ARW model with three different PBL configurations.

2. Data, Methods and Experimental Design

2.1. Observations

BT data of Hurricane Otto from the US National Hurricane Center [3] provides information on the system's position in degrees north and west, maximum sustained winds in knots, central pressure in millibars, category according to the Saffir-Simpson Scale, date and UTC hour of the report. Data are listed every 6 h, and they also include the landfall point in southern Nicaragua (10 n mi northwest of the Nicaragua-Costa Rica border, 1730 UTC 24 November) and the last best-track point before entering the eastern North Pacific basin (0330 UTC 25 November).

2.2. Detecting Rapid Intensification and Tropical Storm Track

Kaplan et al. [19] developed the RI Index (RII) for the Atlantic and the eastern North Pacific basins. This index uses atmospheric and oceanic large-scale predictors that behave differently in each basin. In this study the RII is adapted to be used with modelled data only. The RII uses the criterion proposed by Kaplan and DeMaria [7], which is to consider the change of at least 25 knots (12.9 m s^{-1}) in surface wind in a 24-h period (ΔV_{24}) as a way to determine if the hurricane simulated with WRF-ARW undergoes RI. Furthermore, since RI is not estimated in WRF-ARW output, three large-scale predictors are used here in a similar way to Kaplan et al. [19] for the Atlantic basin, to estimate the probability of RI over the succeeding 24 h utilising linear discriminant analysis from the model output. The chosen large-scale predictors are the vertical wind shear between 850 and 200 hPa (SHRD), horizontal wind divergence at 200 hPa (D200) averaged within a radius of 100 km from the storm centre, and previous 12-h change in intensity of the surface wind (PER). In order to determine the TC track, we select five criteria based on Diro et al. [36]:

- The relative vorticity at 850 hPa must be greater than 1.0×10^{-5} s^{-1}.
- There must be a closed pressure minimum within the radius of 100 km. This minimum pressure is then defined as the centre of the cyclone. Note that use of a 100 km radius improves the TC distribution near the coasts.

- The minimum surface pressure satisfying the above criteria is at least 2 hPa lower than the averaged surface pressure over the surrounding 35 × 35 grid boxes, each with a resolution of 105 km.
- The 10-m surface wind speed must exceed 17.5 m s^{-1}.
- The total tropospheric temperature anomaly calculated by the sum of temperature anomalies at 700, 500 and 300 hPa around the centre of the cyclone must be greater than zero.

2.3. Experimental Design

A set of three numerical experiments are performed to analyse the estimations of RI and trajectory of Hurricane Otto (Table 1) in WRF-ARW with different PBL parameterizations. Each experiment uses a specific PBL scheme: MRF, MYJ and YSU (Medium Range Forecast, Mellor-Yamada-Janjic, and Yonsei University schemes, respectively). Details of each of these parameterizations are briefly described below. We use the regional model WRF-ARW with boundary and initial conditions provided by the GFS analysis (horizontal resolution of 0.5 degrees). The regional model is run in three static domains with horizontal grid spacing of 27, 9 and 3 km as in Figure 3. The finest domain (d03) fully covers the spatial extent of Hurricane Otto during the whole simulation period. The 3-km domain is not configured with cumulus parameterization. It is known that deepest and strongest convective towers are approximately resolved in resolutions higher than 9 km. The model uses 43 vertical levels. Sensitivity tests were not conducted to choose a particular set of physics. The physical parameterization and vertical levels are based on previous operational configurations of HWRF [37]. Some physical options, nevertheless, only work either on WRF-ARW or HWRF. Our goal is to evaluate the regional model performance in the most realistic setup, including aspects such as a topography, coastal geometry, air-land-sea interaction in the complex region of southern Central America. In this respect, the coarse resolution and numerical schemes of GFS do not provide the same level of reliable detail compared to WRF-ARW. Furthermore, in this region meteorological information at high resolution scales is extremely valuable for authorities and decision makers, especially for preparation and mitigation to extreme events such as Hurricane Otto. As mentioned before, landfalling of tropical cyclones in Central America are associated with remarkable socioeconomic impacts, which is relevant for emergency preparedness. Therefore, results are analysed the results at the smaller grid scale for the forecasts of the cyclones' track and intensity as they move into zones with high levels of exposure and vulnerability.

It should be mentioned as well that the coarser domains are only used as a numerical transition of the meteorological information from GFS to forcing the 3-km domain. In addition, many previous studies [33–35,38–42] show that very high resolution simulations (≈3 km or less grid spacing) are useful for representing appropriately the RI and trajectory of tropical cyclones. Therefore, this study uses a 3:1 grid ratio for the nested domains and only analyses the results for the 3-km grid.

Therefore, the model is configured with the following set of physical parameterizations: Eta-Ferrier [43] for microphysics, Dudhia shortwave radiation [44] and RRTM longwave radiation (Rapid Radiative Transfer Model, Mlawer et al. [45]), the unified Noah land-surface model [46], Kain-Fritsch [47] for cumulus parameterization. The surface layer (SL) parameterizations used for the MRF, MYJ and YSU experiments are the fifth-generation Pennsylvania State University–National Center for Atmospheric Research Mesoscale Model (MM5, Grell et al. [48]) similarity [17], Monin-Obukhov [49], and revised MM5 [50] schemes, respectively.

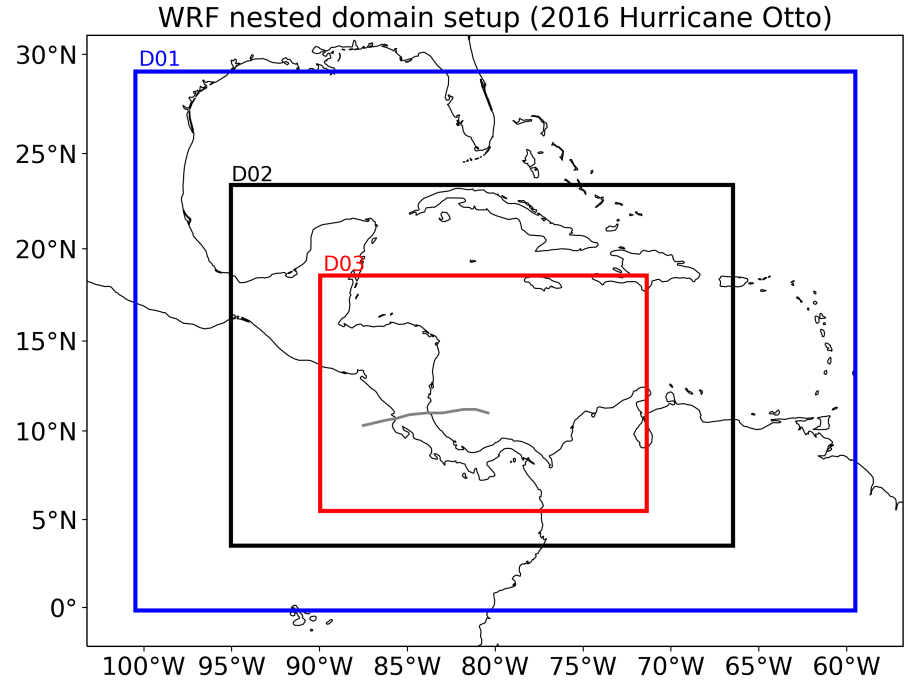

Figure 3. Domain configuration for the simulations of Hurricane Otto using WRF-ARW. The horizontal resolution is 27, 9 and 3 km for domains D01 (blue), D02 (black), and D03 (red). The grey line shows the storm track from the observations during the simulation period from 1200 UTC 23 November 2016 to 1200 UTC 25 November 2016.

Table 1. Experiments carried out to study the intensification and trajectory of Hurricane Otto in the WRF-ARW using different planetary boundary layer (PBL) schemes. SST is not updated in the simulations. CRUN_MRF, EX01_MYJ, and EX02_YSU are: the control-run using the Medium Range Forecast (MRF), the Mellor-Yamada-Janjic (MYJ) and the Yonsei University (YSU) schemes, respectively, in conjunction with their respective surface layer parameterization (SLP). Comparison of storm track dispersion and forward speed between simulations and observations of Hurricane Otto. The observations are taken from Best Track database provided by Brown [3]. Observed forward speed was 4.7 m s^{-1}. The simulations are started on 1200 UTC 22 November 2016 to allow 1-day spinup in the simulation. The analysis period is from 1200 UTC 23 November 2016 to 1200 UTC 25 November 2016.

Experiment	Spinup	PBL	SL	Mean Distance (°)	Forward Speed (m s^{-1})
GFS				0.7	4.8
CRUN_MRF	1-day	MRF	Similarity	1.4	6.4
EX01_MYJ	1-day	MYJ	Monin-Obukov	0.9	5.9
EX02_YSU	1-day	YSU	revised MM5	0.8	5.5

PBL Parameterizations in WRF

MRF Scheme: Hong and Pan [51] described the MRF PBL parameterization. It is commonly used as the default scheme in circulation and forecast models, and in regional models such as MM5 and WRF. MRF uses a non-local PBL approach based on the concept by Troen and Mahrt [52]. The turbulent diffusivity is calculated from a prescribed profile shape as a function of PBL heights and scale parameters derived from similarity requirements. In addition to the advantage in matching conditions between the surface-layer top and the Ekman-layer bottom, it gives the ideal turbulent diffusivity profile, which is based on the physical coupling that the profile and its first derivative be continuous with height and matches the similarity requirements at the surface. Troen and Mahrt [52] pointed out that the non-local approach was promising because it tended to transport moisture away from the surface more rapidly than the local approach. Additionally, using a non-local scheme

improves the precipitation forecast due to enhanced convective overturning at the right location and suppression of spurious rainfall.

Mellor-Yamada-Janjic Scheme (MYJ): this parametrization is a local, level-2.5 closure (i.e., the scheme solves a prognostic equation for Turbulent Kinetic Energy or TKE) as defined by Mellor and Yamada [53]. This scheme is formed by a viscous sublayer, which is allowed to operate only over water. On land, a soil slab of finite depth is used to describe the evolution of the variables at the lower boundary. The surface fluxes are estimated from the mean representative values of the slab. There are two distinct layers: (i) a thin viscous sublayer immediately above the surface, where the vertical transports are determined entirely by the molecular diffusion, and (ii) a turbulent layer above it, where the vertical transports are defined entirely by the turbulent fluxes. The viscous sublayer over the oceans is assumed to operate in three different regimes: (i) smooth and transitional, (ii) rough, and (iii) rough with spray, depending on the roughness Reynolds number. In the Mellor-Yamada level-2.5, the excessive TKE is dissipated rather than producing it at the PBL spinup as in MYJ [49].

Yonsei University Scheme (YSU): Hong et al. [54] described a scheme which is a modification of a previous MRF scheme. The formula keeps the basic concept of Hong and Pan [51] being a non-local PBL scheme, but includes an asymptotic entrainment flux term at the inversion layer. The PBL height (h) is defined as the level in which minimum flux exists at the inversion level, while in Hong and Pan [51] it is the explicit treatment of the entrainment processes through the asymptotic entrainment flux term, whereas the entrainment is implicitly parameterized by raising h above the minimum level flux level in Hong and Pan [51]. As in Hong and Pan [51], above the mixing layer, a local diffusion approach is applied to account for free atmosphere diffusion. The major concept of an explicit treatment of entertainment at PBL top from Noh et al. [55] is adapted. The moisture effect, including water vapour and hydrometeors in the atmosphere, was not taken into account in turbulent mixing. The new concept was devised at large eddy simulation (LES) resolution of a few tens of meters in the vertical. It is found that the YSU PBL scheme produces a realistic structure of the PBL in response to an idealised daytime variation of surface heat and moisture fluxes. The magnitude of the non local mixing terms is smaller than that of the MRF PBL, and plays a role in neutralising the structure of that layer, whereas the non local flux in the MRF PBL produces an overstable structure.

3. Results

Figure 4 shows the storm track from BT data (observations), GFS and experiments with WRF. This figure reveals that, compared to GFS, the regional model simulations better capture the observed location of Otto at the beginning of the simulation period (1200 UTC 23 November). In the WRF simulations, however, the TC travels to the northwest to a maximum latitude of approximately 12° N, and then it turns southwest. This behaviour is similar to what was observed in BT, and this veer is probably due to friction forces at the surface and the presence of a cold surge from the north during those days. GFS failed to represent this particular feature of the hurricane track.

Another relevant feature observed in Figure 4 is the relative acceleration of each storm's simulation as compared to BT. When the TC is over the Pacific Ocean (approximately on 25 November), the WRF simulations and GFS differ from observations significantly. It should be noticed that the algorithm is not detecting Otto in the GFS model on and after 0600 UTC 25 November. Table 2 shows the metrics used to compare the modelled trajectories against BT data. The TC trajectory and forward speed in the GFS are closer to observations; however, after 2300 UTC 24 November, the cyclone in GFS increases its mean forward speed to 8.5 m s^{-1}. Furthermore, as shown in Figure 4, the mean distance to the observed trajectory increases to 1.1 degrees in GFS. On the other hand, in the WRF simulations, EX02_YSU shows better agreement relative to the observations, with a mean distance of 0.8 degrees and a forward speed of 5.5 m s^{-1}. CRUN_MRF shows the worst performance, with the highest mean distance (1.4 degrees) and faster forward speed (6.4 m s^{-1}).

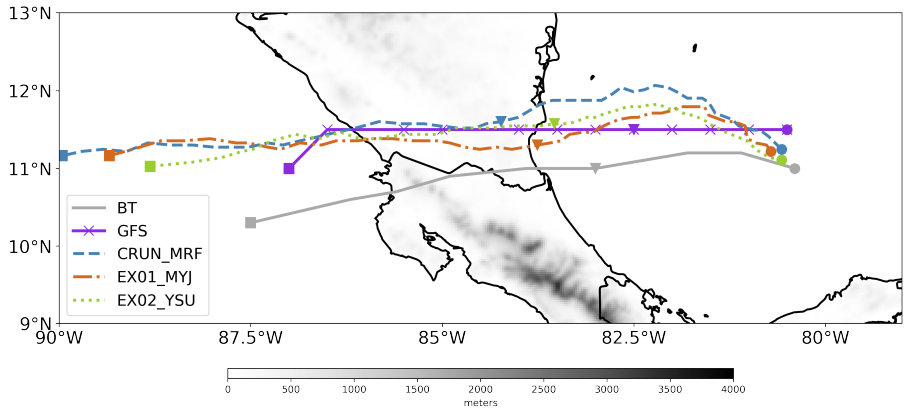

Figure 4. Hurricane Otto storm track for the period 1200 UTC 23 November 2016 to 1200 UTC 25 November 2016 from Best Track (solid line), GFS (solid line with crosses), CRUN_MRF (dashed line), EX01_MYJ (dash-dot line) and EX02_YSU (dotted line). The circle, triangle and square symbols identify the 1200 UTC from 23 to 25 of November 2016. CRUN_MRF, EX01_MYJ, and EX02_YSU are: the control-run using the Medium Range Forecast, the Mellor-Yamada-Janjic and the Yonsei University schemes, respectively. The grey shades represent topography from the 3-km domain.

Figure 5 presents the evolution of Otto during the period of analysis. According to the BT data, by 1200 UTC 23 November this hurricane was category 1 with a maximum sustained wind of 60 knots (30.9 m s^{-1}). At this time GFS underestimated the maximum sustained wind (40 knots or 20.6 m s^{-1}). Experiments CRUN_MRF and EX01_MYJ are closer to the observations with maximum sustained winds of about 60 knots (same hurricane category as in BT). In GFS the hurricane development is not well captured since it reaches category 1 (60-knot wind) by 1500 UTC 24 November. Nevertheless, the timing and value of the sea level pressure (SLP) minimum was better estimated by GFS (about 980 hPa as compared to 975 hPa in BT data). Once the maximum surface wind was reached, the storm weakened afterward, as shown by the decrease in the surface wind speeds in GFS.

WRF simulations improve the evolution of Hurricane Otto as compared to GFS. CRUN_MRF and EX01_MYJ show better agreement with the observations during the first 6 h of simulation, while EX02_YSU overestimates by 20 knots (10.3 m s^{-1}) the maximum surface wind during this period (see Figure 5). Intensification of the TC is remarkably different in each experiment, being quite less in CRUN_MRF, and stronger in EX02_YSU, with a surface wind speed increase of about 20 and 25 knots (10.3 and 12.9 m s^{-1}), respectively. In EX01_MYJ and EX02_YSU, Otto starts to intensify by 0000 UTC 24 November and reaches its maximum at 0300 UTC and 0600 UTC, respectively. In both cases, this intensification occurs before the maximum of surface wind speed in BT data. In these same runs the surface wind decays on and after 1200 UTC 24 November, approximately. By this time, the observations show the maximum intensity and subsequent weakening of Otto. In the case of CRUN_MRF, the maximum surface wind does not experience abrupt changes nor intensify during the simulation period (maximum speeds increased less than 20 knots). It should be noted that only EX02_YSU achieved category 2 before landfall. CRUN_MRF and EX01_MYJ present a weaker TC structure.

When comparing the modelled and observed SLP and surface wind speed time series in Figure 5, it can be noticed that the modelled surface wind speed maximum and the SLP minimum are out of phase. This is contrary to observations, where both events are nearly simultaneous. However, note that the temporal resolution of the BT data is lower, which makes comparison difficult. In GFS, the SLP minimum is seen around 1200 UTC 24 November, while the surface wind maximum occurs later, at 1500 UTC. CRUN_MRF shows a SLP minimum similar to that in GFS, approximately 980 hPa, which takes place 1 h before the surface wind maximum. Meanwhile, the SLP minimum values in EX01_MYJ and EX02_YSU (approximately 970 hPa and 955 hPa, respectively) are lower than those in BT and GFS. In addition, the SLP minimum in both experiments is found approximately 6 h after the

surface wind maxima. These time-lags, which are present in all the regional simulations, suggest that there is a mass-adjustment problem in the simulations, apparently related to the PBL physics and surface layer physics in the model. Differences in surface friction between sea and land as Hurricane Otto approached land may also play a relevant role in the adjustment process.

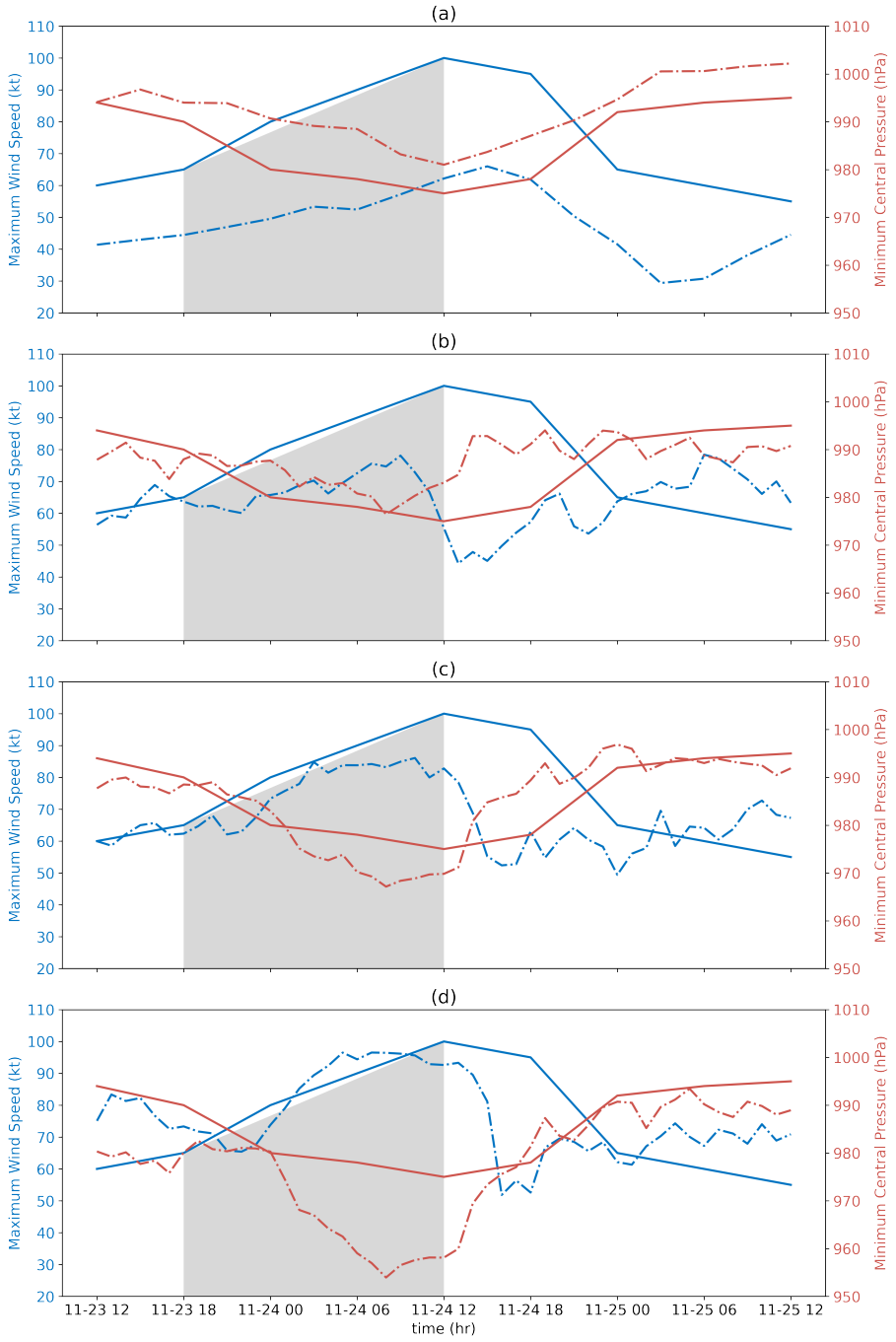

Figure 5. Comparison of Hurricane Otto evolution in terms of maximum surface wind speed (blue lines) and SLP (red lines) as detected in Best Track (solid lines, (**a**) GFS) and experiments (dashed lines, (**b**) CRUN_MRF, (**c**) EX01_MYJ, (**d**) EX02_YSU). Shaded area shows the rapid intensification (RI) period in Best Track (BT).

Landfall point estimations are shown in Table 2. In the BT data, Otto entered Nicaragua at the coordinates 11° N, 83.7° W, on 1642 UTC 24 November. It was a H3 hurricane with maximum sustained wind of 100 knots (50 m s^{-1}), and a forward speed of 8.3 m s^{-1}. In the global and regional models

the landfall location is close to the observations; however, they differ significantly in timing. GFS and EX02_YSU landfall occurs at a later time, while in CRUN_MRF and EX01_MYJ it is earlier. Also, forward speed is consistently underestimated (by about 2 m s^{-1}) in all models, as compared to the BT data. Meanwhile, SLP values were relatively close to observations in the WRF simulations and GFS. Maximum sustained wind speed, related to hurricane category, was underestimated in both the GFS and WRF experiments. During landfall, Otto had hurricane category only in the WRF simulations (H1 in CRUN_MRF and EX01_MYJ, and H2 in EX02_YSU).

Table 2. Landfall measurements of Hurricane Otto from Best Track database and simulation using the WRF-ARW modelling system. Storm categories are taken from the Saffir-Simpson hurricane wind scale. GFS is the Global Forecasting System model. CRUN_MRF, EX01_MYJ, and EX02_YSU are: the control-run using the Medium Range Forecast, the Mellor-Yamada-Janjic and the Yonsei University schemes, respectively. The columns are DFOL: distance from observed landfall in degrees, FS: forward speed (m s^{-1}), T: Time (UTC), P: pressure (hPa), MWS: maximum wind speed (m s^{-1}) and Cat: Saffir-Simpson scale.

Data	Lon.	Lat.	DFOL	FS	T	P	MWS	Cat.
Obs.	−83.7	11.0		8.3	16:42	975	50	3
GFS	−83.8	11.5	0.5	5.4	23:05	993	22	TS
CRUN_MRF	−83.7	11.8	0.8	5.3	09:51	980	37	1
EX01_MYJ	−83.9	11.3	0.4	5.3	13:40	978	36	1
EX02_YSU	−83.8	11.6	0.6	5.8	23:11	971	44	2

Table 3 shows the metrics and indices used to estimate the RI in all models. These indices are based on the study by Kaplan et al. [19], and adapted to high resolution models. As presented in this table, only GFS and EX01_MYJ are close to the 25-knot intensity change threshold and the hurricane attains category 1 intensity. CRUN_MRF is not showing a significant increase in wind speed and the TC does not reach hurricane category before landfall. In experiment EX02_YSU the simulated Hurricane Otto intensifies to category 2, but it does not undergo a RI process. Even though the MYJ experiment was the only one that exhibited an abrupt 24-h change in the storm's surface wind, close to the 25-knot threshold, the YSU scheme presented the fastest intensification, closest to reality. PER indices are of the same order of magnitude to those of Kaplan et al. [19] except for CRUN_MRF, which is negative. In all the WRF experiments, D200 is one order of magnitude lower than in Kaplan et al. [19]. This marked difference could be due to the different radii used to estimate these indices in this study, but also to the fact that none of the simulations is capturing the RI process of Hurricane Otto. SHRD in all the experiments has similar values to those reported by Kaplan et al. [19] for non RI hurricanes.

As explained above, the main difference amongst these PBL schemes is the way the vertical fluxes are estimated in this layer. The default configuration of MRF PBL scheme using a non-local estimation of turbulent diffusivity, shows deficiencies even in the estimation of the hurricane development, since the TC in this experiment only reaches category 1 in short and intermittent periods of its evolution (not shown). In the other two PBL schemes, MYJ and YSU, the TC development is more defined and persistent. The cyclone reaches a category 2; however, as mentioned, the hurricane did not undergo RI in either case. The YSU is a sophisticated non-local scheme based on MRF formulation, which improves the entrainment fluxes and non-local terms compared to MRF, however, this enhancement is not enough to capture Hurricane Otto RI. Moreover, the MYJ scheme is a level-2.5 approximation of TKE, that shows better estimation of landfall and RI compared to the other two simulations.

Table 3. Mean magnitudes of RI predictors estimated for the Hurricane Otto observations and simulations using the GFS and WRF-ARW model for the 25-knot threshold. GFS is the Global Forecasting System model. CRUN_MRF, EX01_MYJ, and EX02_YSU are: the control-run using the Medium Range Forecast, the Mellor-Yamada-Janjic and the Yonsei University schemes, respectively. The columns are WS: wind speed (m s^{-1}), Cat: Saffir-Simpson scale, ΔV_{24}: change in the surface wind in at least 24-h (m s^{-1}), PER: previous 12-h change in intensity of the surface wind (m s^{-1}), D200: horizontal wind divergence at 200 hPa (1×10^{-5} s^{-1}) and SHRD: the vertical wind shear between 850 and 200 hPa (m s^{-1}).

Data	Date	Lon.	Lat.	WS	Cat.	ΔV_{24}	PER	D200	SHRD
Obs.	2016-11-24 12:00:00	−83.0	11	52	3	40	10		
GFS	2016-11-24 15:00:00	−83.0	11.5	33	1	22	6		
CRUN_MRF	2016-11-24 12:00:00	−82.4	12	33	TS	−1	−5	1	11
EX01_MYJ	2016-11-24 12:00:00	−83.6	11.3	42	1	23	5	8	8
EX02_YSU	2016-11-24 12:00:00	−83.4	11.6	46	2	16	9	9	10

4. Discussion

Despite the fact that southern Central America is rarely affected by the direct landfall of tropical cyclones, historic observational records showed that at least three cases, Tropical Storm 19 in 1887, Martha in 1969, and Otto in 2016, reached the southernmost countries of this region. It is very important to investigate the ability of state-of-the-art regional and mesoscale models to represent the most relevant characteristics of these tropical cyclones at relatively low latitudes, because they are associated with remarkable socio-economic impacts and even loss of lives. Identifying these critical characteristics is relevant for emergency preparedness. For example, forecasts of the cyclones' track and their intensity as they move into zones with high levels of exposure and vulnerability help the local and regional emergency agencies to send adequate alerts to potentially affected communities.

To explore the ability of regional models to capture the RI and trajectory of extreme events such as Hurricane Otto, a set of three high resolution simulations using the regional model WRF-ARW with different PBL schemes were performed and evaluated for this particular tropical cyclone. GFS data with horizontal resolution of 0.5 degrees were used as initial and boundary conditions. A triple-nested domain configuration with horizontal resolutions of 27, 9, and 3 km was used in the experiments.

By and large the simulations improve the results as compared to the GFS data, in almost every aspect evaluated in this study. Particularly, trajectories in the simulations show a better representation of the direction of movement. Initially, the cyclone was heading to the northwest but then moved to the southwest, mainly due to the friction forces and the influence of an arriving cold surge from the north of the continent [12]. Forward speed in GFS was on average in better agreement with observations, but in the simulations hurricane Otto moved faster. This suggests some influence of the PBL schemes in both the interaction of the cyclone with friction forces at the surface and the input and exchange of momentum and energy from the water surface through turbulent processes.

Physical processes in the development, decay, and movement of TCs are affected by many factors such as SST, low-level moisture flux convergence, vertical wind shear, distribution of vertical motion, among others, in such a way, that the role of surface friction over sea or land can vary enormously depending on the tropical cyclone features [56]. The complexity of the problem during TC landfalling is even bigger when horizontal gradients of surface friction between land and sea are considered. According to Wong and Chan [57], who performed numerical experiments with the MM5 model, land surface friction dominates surface-moisture flux over land, which is apparently essential for the movement of TC toward land. The final drift of a TC depends then on many elements whose dynamics and thermodynamics are not clearly understood. Yuan et al. [58] used the quasi-geostrophic barotropic vorticity equation model to simulate the influence of surface friction on TC track and intensity. One of their results, relevant to this study, is that land friction may be relevant in causing sudden drifts in TC track near landfalling. In the case of Otto, the category of the cyclone was H3 before landfalling,

suggesting a strong surface friction gradient between sea and land that may have caused the southwest deflection of this disturbance. The fact that GFS shows a westward track over land and our results improve Otto's track toward the southwest as observed, may be caused by the finer resolution and more realistic surface physical parameterizations in WRF than in GFS. Another factor usually not considered in most numerical experimental work of TC movement after its landfalling, is the effect of friction due to the shape of the coast. As can be judged from Figures 1a and 3, the coastal contour where Otto entered suggests a complex surface friction interaction with the nonsymmetric Otto's vortex as observed in Figure 2. This asymmetry was also evident in the lightning distribution of this cyclone using World Wide Lightning Location Network data [8].

Current knowledge of low-level physical processes is clear about the role of surface friction, moisture flux, kinetic energy exchanges, and others, in the evolution and intensification of TC. Shin et al. [59] compared five PBL schemes using the WRF model during a field program. As part of the experimental design they tested two of the parameterizations used in this work, the YSU (first-order), and MYJ (TKE) closure schemes. An important result of their work, regarding PBL, is that, "surface-layer formulations only contribute to near-surface variability and then PBL mean properties, whereas shapes of the profiles are determined by PBL mixing algorithms". This outcome, if applicable under more turbulent TC conditions, may mean that our results using both schemes would not diverge much from observed data since, the MYJ experiment exhibited an abrupt 24-h change in the storm's surface wind, close to the 25-knot threshold specified here, and the YSU scheme presented the fastest intensification, closest to reality. As observed in Figure 4, orography near Otto landfalling is composed of relatively very low hills presumably not affecting much TC decay. Lee et al. [60] tested if subgrid-scale topography schemes adequately simulated the surface layer wind using the WRF at a high-resolution of 3 km, the same grid size used in this work. A result of interest to this paper is that when using the orography parameterization, the wind speed decreased over relatively flat regions, as those of northern Costa Rica and southern Nicaragua. At this point, more research needs to be done to address the question, what is more relevant for TC surface wind evolution over land, the surface friction or the parameterization of orography? In our case, it seems that surface friction may be more important to resolve, since in our experimental design no orography parameterization was used. Recently, Wang et al. [61] made a sensitivity analysis on the level of land-atmosphere coupling to the surface layer using the WRF and a YSU scheme by perturbing the parameters of this representation of the PBL. This work offers a different methodological approach other than to alter two different physics components in the model. One important result of Wang et al. [61] is that perturbing parameters in that scheme, can cause large simulation uncertainties comparable to those in the observations. Since observations are deficient in most tropical cyclones, especially in Otto in Central America, altering two or more physics elements of the model would not provide more information than that of the results obtained here, especially in regard to their uncertainty properties.

Landfall results did not show significant differences amongst GFS and the experiments. Furthermore, all the estimations missed the landfall timing, with EX01_MYJ being closest to the observations. Regarding RI, EX01_MYJ was the only experiment that exhibited an abrupt 24-h change in the storm's surface wind, close to the 25-knot threshold, but Hurricane Otto did not reach category 3 intensity in this simulation. In conclusion, according to the results from this study, the level-2.5 turbulent kinetic enegy based PBL schemes such as MYJ are more suitable for representing the processes of development and some features of the structure of Hurricane Otto. As noted before, impacts over Costa Rica and Nicaragua, due to precipitation, winds, and low-level pressures associated with Otto, before and after landfall, brought severe damage and loss of lives in both countries. Future work, assessing model simulation data against local surface and upper air observations, radar and lightning data would most probably improve our knowledge of how these models represent the distribution of those variables over land.

5. Conclusions

This study allowed to examine the performance of WRF-ARW using three different planetary boundary layer parameterizations in the estimation of Otto's trajectory and the RI process. Our results, using this regional model with a finer resolution than that of the GFS, along with the MRF, MYJ and YSU parameterization schemes, the latter resulting in the fastest intensification closest to reality, provide a potential forecasting tool to improve movement rate and track of TC near landfalling.

Trajectories in the simulations show a better representation of the direction of movement. Forward speed in GFS was on average in better agreement with observations, but in the simulations Hurricane Otto moved faster, maybe due to surface layer properties and friction not being represented realistically in the parameterization schemes used.

Landfall results did not show significant differences amongst GFS and the experiments, furthermore, all the estimations missed the landfall timing, with MYJ being closest to the observations.

Author Contributions: Conceptualization, T.M., J.A.A. and E.R.R.; methodology, T.M., J.A.A. and E.R.R.; software, T.M.; validation, T.M., J.A.A. and E.R.R.; formal analysis, T.M., J.A.A., E.R.R., H.G.H. and E.J.A.; investigation, T.M.; resources, J.A.A., H.G.H. and E.J.A.; data curation, T.M.; writing—original draft preparation, T.M.; writing—review and editing, T.M.; visualization, T.M.; supervision, T.M. and J.A.A.; project administration, T.M. and J.A.A.; funding acquisition, J.A.A., E.J.A. and H.G.H. All authors have read and agreed to the published version of the manuscript.

Funding: This research was funded by the projects B9-454 (VI-Grupos), B8-766 (VI-Redes), B8-604 and B9-609 (Fondo de Estímulo), EC-497 (FEES-CONARE), C0-074, B0-810 and C0-610 (Fondo de Estímulo), from the Center for Geophysical Research (CIGEFI) of the UCR.

Acknowledgments: T.M. would like to thank Anna Rutgersson for the internship at Uppsala University to develop part of this research. J.A.A., E.R., H.G.H. and E.J.A. thank to the UCR School of Physics for giving us the research time to develop this study. To the UCR research center CIGEFI for their logistic support during the data compilation and analysis.

Conflicts of Interest: The authors declare no conflict of interest.

References

1. Peña, M.; Douglas, M.W. Characteristics of Wet and Dry Spells over the Pacific Side of Central America during the Rainy Season. *Mon. Weather Rev.* **2002**, *130*, 3054–3073. [CrossRef]
2. Hidalgo, H.G.; Alfaro, E.J.; Hernández-Castro, F.; Pérez-Briceño, P.M. Identification of Tropical Cyclones' Critical Positions Associated with Extreme Precipitation Events in Central America. *Atmosphere* **2020**, *11*, 1123. [CrossRef]
3. Brown, D.P. *Hurricane Otto (AL162016, EP22016): 20–26 November 2016*; Technical Report; National Hurricane Center: Miami, FL, USA, 2017.
4. Simpson, R.H.; Hope, J.R. Atlantic Hurricane Season of 1971. *Mon. Weather Rev.* **1972**, *100*, 256–267. [CrossRef]
5. Díaz-Bolaños, R.E. La tormenta tropical de 1887 y su paso por las fuentes históricas costarricenses. *Estudios* **2004**, 39–56. [CrossRef]
6. Simpson, R.H.; Sugg, A.L. The Atlantic hurricane season of 1969. *Mon. Weather Rev.* **1970**, *98*, 293–306. [CrossRef]
7. Kaplan, J.; DeMaria, M. Large-Scale Characteristics of Rapidly Intensifying Tropical Cyclones in the North Atlantic Basin. *Weather Forecast.* **2003**, *18*, 1093–1108. [CrossRef]
8. Arce-Fernández, D.; Amador, J.A. Actividad eléctrica asociada al huracán Otto (2016) en el Mar Caribe y en el Corredor Seco Centroamericano. *Rev. Bras. Meteorol.* **2020**, *35*, in press.
9. Knapp, K.R.; Kossin, J.P. New global tropical cyclone data set from ISCCP B1 geostationary satellite observations. *J. Appl. Remote Sens.* **2007**, *1*, 013505. [CrossRef]
10. Amador, J.A.; Hidalgo, H.G.; Alfaro, E.J.; Durán-Quesada, A.M.; Calderón, B.; Mora, N.; Arce, D. Central America [in "State of the Climate in 2016"]. *Butt. Am. Meteorol. Soc.* **2017**, *98*, Si-S280. [CrossRef]
11. IMN. *Huracán Otto: Informe Técnico*; Technical Report; Instituto Meteorógico Nacional: San José, Costa Rica, 2017.

12. Chinchilla-Ramírez, M.G. *Resumen Meteorológico Noviembre 2016*; Technical Report; Instituto Meteorógico Nacional: San José, Costa Rica, 2016.
13. Alfaro, E.J.; Hidalgo, H.G.; Maldonado, T.; Pérez-Briceño, P.M.; Mora, N.P. A Tri-dimensional Approach to Climate Sciences. *Caribb. Q.* **2018**, *64*, 26–56. [CrossRef]
14. Quesada-Román, A.; Fallas-López, B.; Hernández-Espinoza, K.; Stoffel, M.; Ballesteros-Cánovas, J.A. Relationships between earthquakes, hurricanes, and landslides in Costa Rica. *Landslides* **2019**, *16*, 1539–1550. [CrossRef]
15. Quesada-Román, A.; Villalobos-Chacón, A. Flash flood impacts of Hurricane Otto and hydrometeorological risk mapping in Costa Rica. *Geogr. Tidsskr.* **2020**, 1–14. [CrossRef]
16. Poleo, D.C.V.; Stoltz, W. Comparación y evaluación de diferentes esquemas de parametrización de cúmulus con el WRF EMS aplicadas al huracán Otto. *Top. Meteorol. Oceanogr.* **2017**, *16*, 28–40.
17. Grell, G.A.; Freitas, S.R. A scale and aerosol aware stochastic convective parameterization for weather and air quality modeling. *Atmos. Chem. Phys.* **2014**, *14*, 5233–5250. [CrossRef]
18. Skamarock, W.C.; Klemp, J.B.; Dudhia, J.; Gill, D.O.; Barker, D.M.; Duda, M.G.; Huang, X.Y.; Wang, W.; Powers, J.G. *A Description of the Advanced Research WRF Version 3*; NCAR Tech. Note NCAR/TN-475+ STR; NCAR: Boulder, CO, USA, 2008.
19. Kaplan, J.; DeMaria, M.; Knaff, J.A. A Revised Tropical Cyclone Rapid Intensification Index for the Atlantic and Eastern North Pacific Basins. *Weather Forecast.* **2010**, *25*, 220–241. [CrossRef]
20. Klotzbach, P.J. El Niño-Southern Oscillation, the Madden-Julian Oscillation and Atlantic basin tropical cyclone rapid intensification. *J. Geophys. Res.-Atmos.* **2012**, *117*, D14104. [CrossRef]
21. Wang, C.; Wang, X.; Weisberg, R.H.; Black, M.L. Variability of tropical cyclone rapid intensification in the North Atlantic and its relationship with climate variations. *Clim. Dynam.* **2017**, *49*, 3627–3645. [CrossRef]
22. Knabb, R.D.; Rhome, J.R.; Brown, D.P. *Hurricane Katrina (AL122005): 23–30 August 2005*; Technical Report; National Hurricane Center: Miami, FL, USA, 2005.
23. McTaggart-Cowan, R.; Bosart, L.F.; Gyakum, J.R.; Atallah, E.H. Hurricane Katrina (2005). Part I: Complex Life Cycle of an Intense Tropical Cyclone. *Mon. Weather Rev.* **2007**, *135*, 3905–3926. [CrossRef]
24. Pasch, R.J.; Penny, A.B.; Berg, R. *Hurricane María (AL 152017), 16–30 September 2017*; Technical Report; National Hurricane Center: Miami, FL, USA, 2018.
25. Klotzbach, P.J.; Carl, J.; Schreck, C.J., III; Collins, J.M.; Bell, M.M.; Blake, E.S.; Roache, D. The Extremely Active 2017 North Atlantic Hurricane Season. *Mon. Weather Rev.* **2018**, *146*, 3425–3443. [CrossRef]
26. Charney, J.G.; Eliassen, A. On the Growth of the Hurricane Depression. *J. Atmos. Sci.* **1964**, *21*, 68–75. [CrossRef]
27. Ogura, Y. Frictionally Controlled, Thermally Driven Circulations in a Circular Vortex with Application to Tropical Cyclones. *J. Atmos. Sci.* **1964**, *21*, 610–621. [CrossRef]
28. Ooyama, K. Numerical Simulation of the Life Cycle of Tropical Cyclones. *J. Atmos. Sci.* **1969**, *26*, 3–40. [CrossRef]
29. Emanuel, K.A. An Air-Sea Interaction Theory for Tropical Cyclones. Part I: Steady-State Maintenance. *J. Atmos. Sci.* **1986**, *43*, 585–605. [CrossRef]
30. Emanuel, K.A. The Behavior of a Simple Hurricane Model Using a Convective Scheme Based on Subcloud-Layer Entropy Equilibrium. *J. Atmos. Sci.* **1995**, *52*, 3960–3968. [CrossRef]
31. Emanuel, K.A. Some Aspects of Hurricane Inner-Core Dynamics and Energetics. *J. Atmos. Sci.* **1997**, *54*, 1014–1026. [CrossRef]
32. Smith, R.K.; Montgomery, M.T.; Vogl, S. A critique of Emanuel's hurricane model and potential intensity theory. *Q. J. R. Meteorol. Soc.* **2008**, *134*, 551–561. [CrossRef]
33. Zhang, J.A.; Nolan, D.S.; Rogers, R.F.; Tallapragada, V. Evaluating the Impact of Improvements in the Boundary Layer Parameterization on Hurricane Intensity and Structure Forecasts in HWRF. *Mon. Weather Rev.* **2015**, *143*, 3136–3155. [CrossRef]
34. Kilroy, G.; Smith, R.K. The effects of initial vortex size on tropical cyclogenesis and intensification. *Q. J. R. Meteorol. Soc.* **2017**, *143*, 2832–2845. [CrossRef]
35. Zhang, J.A.; Rogers, R.F.; Tallapragada, V. Impact of Parameterized Boundary Layer Structure on Tropical Cyclone Rapid Intensification Forecasts in HWRF. *Mon. Weather Rev.* **2017**, *145*, 1413–1426. [CrossRef]

36. Diro, G.T.; Giorgi, F.; Fuentes-Franco, R.; Walsh, K.J.E.; Giuliani, G.; Coppola, E. Tropical cyclones in a regional climate change projection with RegCM4 over the CORDEX Central America domain. *Clim. Chang.* **2014**, *125*, 79–94. [CrossRef]
37. Biswas, M.K.; Carson, L.; Newman, K.; Bernardet, L.; Kalina, E.; Grell, E.; Frimel, J. Available online: https://dtcenter.org/sites/default/files/community-code/hwrf/HWRF_v3.9a_UG.pdf (accessed on 26 November 2020).
38. Li, X.; Pu, Z. Sensitivity of Numerical Simulation of Early Rapid Intensification of Hurricane Emily (2005) to Cloud Microphysical and Planetary Boundary Layer Parameterizations. *Mon. Weather Rev.* **2008**, *136*, 4819–4838. [CrossRef]
39. Chen, H.; Zhang, D.L.; Carton, J.; Atlas, R. On the Rapid Intensification of Hurricane Wilma (2005). Part I: Model Prediction and Structural Changes. *Weather Forecast.* **2011**, *26*, 885–901. [CrossRef]
40. Kilroy, G.; Smith, R.K.; Montgomery, M.T. A unified view of tropical cyclogenesis and intensification. *Q. J. R. Meteorol. Soc.* **2016**, *143*, 450–462. [CrossRef]
41. Kilroy, G.; Montgomery, M.T.; Smith, R.K. The role of boundary-layer friction on tropical cyclogenesis and subsequent intensification. *Q. J. R. Meteorol. Soc.* **2017**, *143*, 2524–2536. [CrossRef]
42. Kilroy, G.; Smith, R.K.; Montgomery, M.T. The role of heating and cooling associated with ice processes on tropical cyclogenesis and intensification. *Q. J. R. Meteorol. Soc.* **2018**, *144*, 99–114. [CrossRef]
43. Rogers, E.; Black, T.; Ferrier, B.; Lin, Y.; Parrish, D.; DiMego, G. National Oceanic and Atmospheric Administration Changes to the NCEP Meso Eta Analysis and Forecast System: Increase in resolution, new cloud microphysics, modified precipitation assimilation, modified 3DVAR analysis. *NWS Tech. Proced. Bull.* **2001**, *488*, 1–15.
44. Dudhia, J. Numerical Study of Convection Observed during the Winter Monsoon Experiment Using a Mesoscale Two-Dimensional Model. *J. Atmos. Sci.* **1989**, *46*, 3077–3107. [CrossRef]
45. Mlawer, E.J.; Taubman, S.J.; Brown, P.D.; Iacono, M.J.; Clough, S.A. Radiative transfer for inhomogeneous atmospheres: RRTM, a validated correlated-k model for the longwave. *J. Geophys. Res.-Atmos.* **1997**, *102*, 16663–16682. [CrossRef]
46. Tewari, M.; Chen, F.; Wang, W.; Dudhia, J.; LeMone, M.A.; Mitchell, K.; Ek, M.; Gayno, G.; Wegiel, J.; Cuenca, R.H. Implementation and verification of the unified NOAH land surface model in the WRF model (Formerly Paper Number 17.5). In Proceedings of the 20th Conference on Weather Analysis and Forecasting/16th Conference on Numerical Weather Prediction, Seattle, WA, USA, 14 January 2004; pp. 11–15.
47. Kain, J.S. The Kain–Fritsch Convective Parameterization: An Update. *J. Appl. Meteorol.* **2004**, *43*, 170–181. [CrossRef]
48. Grell, G.A.; Dudhia, J.; Stauffer, D.R. *A Description of the Fifth-Generation Penn State/NCAR Mesoscale Model (MM5)*; University Corporation for Atmospheric Research: Boulder, CO, USA, 1994.
49. Janjić, Z.I. The Step-Mountain Eta Coordinate Model: Further Developments of the Convection, Viscous Sublayer, and Turbulence Closure Schemes. *Mon. Weather Rev.* **1994**, *122*, 927–945. [CrossRef]
50. Jiménez, P.A.; Dudhia, J.; González-Rouco, J.F.; Navarro, J.; Montávez, J.P.; García-Bustamante, E. A Revised Scheme for the WRF Surface Layer Formulation. *Mon. Weather Rev.* **2012**, *140*, 898–918. [CrossRef]
51. Hong, S.Y.; Pan, H.L. Nonlocal Boundary Layer Vertical Diffusion in a Medium-Range Forecast Model. *Mon. Weather Rev.* **1996**, *124*, 2322–2339. [CrossRef]
52. Troen, I.B.; Mahrt, L. A simple model of the atmospheric boundary layer: Sensitivity to surface evaporation. *Bound.-Layer Meteorol.* **1986**, *37*, 129–148. [CrossRef]
53. Mellor, G.L.; Yamada, T. Development of a turbulence closure model for geophysical fluid problems. *Rev. Geophys.* **1982**, *20*, 851. [CrossRef]
54. Hong, S.Y.; Noh, Y.; Dudhia, J. A New Vertical Diffusion Package with an Explicit Treatment of Entrainment Processes. *Mon. Weather Rev.* **2006**, *134*, 2318–2341. [CrossRef]
55. Noh, Y.; Cheon, W.G.; Hong, S.Y.; Raasch, S. Improvement of the K-profile Model for the Planetary Boundary Layer based on Large Eddy Simulation Data. *Bound.-Layer Meteorol.* **2003**, *107*, 401–427. [CrossRef]
56. Fang, J.; Tang, J.; Wu, R. The effect of surface friction on the development of tropical cyclones. *Adv. Atmos. Sci.* **2009**, *26*, 1146–1156. [CrossRef]
57. Wong, M.L.M.; Chan, J.C.L. Tropical Cyclone Motion in Response to Land Surface Friction. *J. Atmos. Sci.* **2006**, *63*, 1324–1337. [CrossRef]

58. Yuan, J.; Huang, Y.; Liu, C.; Wan, Q. A simulation study of the influence of land friction on landfall tropical cyclone track and intensity. *J. Trop. Meteorol.* **2008**, *14*, 53–56.
59. Shin, H.H.; Hong, S.Y. Intercomparison of Planetary Boundary-Layer Parametrizations in the WRF Model for a Single Day from CASES-99. *Bound.-Layer Meteorol.* **2011**, *139*, 261–281. [CrossRef]
60. Lee, J.; Shin, H.H.; Hong, S.Y.; Jiménez, P.A.; Dudhia, J.; Hong, J. Impacts of subgrid-scale orography parameterization on simulated surface layer wind and monsoonal precipitation in the high-resolution WRF model. *J. Geophys. Res. Atmos.* **2015**, *120*, 644–653. [CrossRef]
61. Wang, C.; Qian, Y.; Duan, Q.; Huang, M.; Berg, L.K.; Shin, H.H.; Feng, Z.; Yang, B.; Quan, J.; Hong, S.; et al. Assessing the sensitivity of land-atmosphere coupling strength to boundary and surface layer parameters in the WRF model over Amazon. *Atmos. Res.* **2020**, *234*, 104738. [CrossRef]